Journal of Textiles and Polymers

Vol. 12, No. 3, 32-46, July 2024
https://www.itast.ir
DOI: https://doi.org/10.48302/jtp.2026.551085.1335

Encapsulation of Zeolite/clindamycin drug into PXDDA/PVA nanofibers to investigate drug delivery

Mohaddeseh Sharifi[1], S.Hajir Bahrami [1*]

[1] Department of Textile Engineering, Amirkabir University of Technology, Tehran, Iran.

Article Information

Article history:

Received: 2025-10-04

Accepted: 2025-02-17

***Keywords*:**

Poly (xylitol-co-dodecanedioic acid) (PXDDA), Zeolite, Clindamycin drug, Nanofibers.

Abstract

This study aimed to develop electrospun nanofibrous based on poly (xylitol-co-dodecanedioic acid) (PXDDA) blended with polyvinyl alcohol (PVA), incorporating clindamycin drug (CD)-loaded zeolite (ZO) particles as a capsule for controlled drug delivery in wound-healing applications. Since PXDDA alone could not be electrospun, PVA was added to achieve suitable viscosity and conductivity. Response Surface Methodology (RSM) was used to optimize electrospinning parameters, resulting in uniform nanofibers with an average diameter of 395 ± 76 nm at 17.07% PXDDA, 10% PVA polymer solutions, voltage 20 kV, and flow rate 0.75 mL/h. Incorporation of clindamycin/ZO capsules at 2/2% and 2/5% (w/w) increased fiber diameter to 545 ± 110 nm and 588 ± 149 nm, respectively, due to higher solution viscosity and capsule entrapment. Crosslinking with glutaraldehyde/HCl vapor enhanced structural stability and influenced hydrophilicity, with centrifuged capsules showing higher contact angles by reducing free drug in the polymer matrix. Drug-release studies demonstrated that centrifuged capsules effectively minimized burst release and enabled sustained release over 48 h, following Higuchi diffusion kinetics. Overall, the optimized PXDDA/PVA nanofibers with centrifuged CD/ZO capsules provide controlled antibiotic delivery and appropriate surface properties for cell attachment, highlighting their strong potential as antibacterial scaffolds for wound healing.

1 INTRODUCTION

Tissue engineering is an emerging biomedical strategy aimed at repairing or regenerating damaged tissues using three-dimensional biomaterials that mimic the extracellular matrix (ECM). Among these, polymeric biomaterials are especially attractive because of their high water content, porous structure, and ability to be tailored as scaffolds that support cell attachment and promote tissue regeneration.[1, 2]. To support tissue regeneration, a biomaterial must provide mechanical properties compatible with the target tissue [3, 4]. Among different methods to fabricate nanofibers, electrospinning is particularly advantageous because it can generate micro- to nanoscale fibers with a high surface area, making it highly suitable for tissue engineering applications [5-7]. Electrospun fibers can be effectively created from a wide range of polymeric materials, with adjustable alignment ratios. Their unique features, such as a highly porous structure, small interconnected pores, and a large surface-to-volume ratio, make electrospun fiber mats a promising option for biomedical and tissue engineering applications. However, certain factors limit their practical use [8]. Among polymeric biomaterials, polyesters are widely used in tissue engineering due to their biocompatibility and biodegradability. However, some polyesters, like poly (lactic acid) (PLA) and poly (caprolactone) (PCL) are produced through complex and costly processes that often involve toxic catalysts, large amounts of organic solvents, and reliance on nonrenewable resources. In contrast, poly (xylitol-co-dodecanedioic acid) (PXDDA) polymer is a polyester synthesized from biocompatible monomers using a simple, cost-effective method, without the need for toxic solvents or excessive catalysts [9].

Xylitol, a natural sugar alcohol with multiple hydroxyl groups, is abundant, inexpensive, safe, and FDA-approved, with additional benefits such as antibacterial activity, anticariogenic effects, and support for bone metabolism. However, because xylitol is water-soluble and lacks structural integrity, it cannot function as a scaffold on its own. To overcome this limitation, it is polymerized with the biocompatible cross-linker dodecanedioic acid (DDA), which creates a stable polymer network. DDA introduces cross-linking sites that improve structural strength and provide beneficial biological functions, making the resulting PXDDA polymer suitable for tissue engineering applications. [9]. Amir Sotoudeh et al worked on the synthesis of copolymer of

* Corresponding author: hajirb@aut.ac.ir

Poly (xylitol-dodecanedioic acid)-co- polylactic acid (PXDDA-co-PLA) with different percentages of bioglass nanoparticles on tissue engineering applications [10]. The higher surface area and fine pores of nanofibers prepared by the electrospinning process provide the high efficient delivery of drugs and could increase the local drug concentration, especially for the treatment of tissues with drug delivery systems [11]. The clindamycin drug has a considerable potential to enhance cell attachment and proliferation, thereby improving extracellular matrix (ECM) components. However, the release rate of drugs released is crucial for maximizing the effectiveness of a drug delivery system [12]. Clindamycin is one of the most ubiquitous and potent antibiotics with broad-spectrum antibiotic activity. It is originally derived from lincomycin. It prevents bacterial protein synthesis by binding to the 50S ribosomal subunit and interfering with transpeptidation, producing a strong bacteriostatic effect against Gram-positive cocci, Gram-negative bacilli, and anaerobic bacteria. Clindamycin has numerous medical applications in the treatment of infections. Also, it has a relatively short half-life upon systemic administration and therefore typically requires administration every 6 h to ensure adequate antibiotic concentrations. Systemic antibiotic therapy has known disadvantages, such as potential systemic toxicity and wound necrosis [13]. Voicu et al investigated CD release from chitosan-hydroxyapatite composite to prevent infections at the implantation site [14]. Nadem et al worked on the crosslinked PVA nanofibers as a drug carrier of CD [15]. Alifah et al evaluated the release of CD from PVA hydrogel for the treatment of infected wounds [16]. Various strategies, including free drug incorporation, encapsulation, and nanocarrier-based delivery, are used to achieve localized drug release in tissue engineering. Because uncontrolled or burst release can reduce therapeutic efficiency, regulating both the amount and duration of release is essential. This control can be achieved by modifying scaffold composition, drug-loading methods, or drug-release systems. Zeolite, a silica-based nanoporous material, is particularly advantageous for controlled and localized delivery due to its low cost, biocompatibility, high surface area, tunable porosity, fast diffusion, and strong mechanical stability. These properties also make zeolite valuable for antibacterial coatings, cosmetics, biosensing, and advanced drug-delivery applications. [17, 18].

Bin Jiang et al worked on the zeolite Y nanoparticles as a carrier for curcumin in PCL-gelatin electrospun nanofibers. Loading curcumin in zeolite nanoparticles was designed to sustain and long-term drug release [19]. Fatemeh Haghdoost used zeolite in polyethersulfone (PES)/polyvinylpyrrolidone (PVP) polymer solution as a composite nanofiber. So, PVP/zeolite (shell) and PES (core) nanofibers were electrospun [20]. Also, Babak Faraji Dizaji worked on the different types of zeolites in PLGA/chitosan polymers solutions for targeted delivery of Paclitaxel toward prostate cancer cells death [11]. In this study, the main objective was to fabricate electrospun nanofibers based on poly(xylitol-co-dodecanedioic acid) (PXDDA) for tissue engineering applications. Since PXDDA alone could not be electrospun, polyvinyl alcohol (PVA) was incorporated to provide the required viscosity and conductivity for fiber formation. Response Surface Methodology (RSM) was used to identify the optimal conditions for producing uniform nanofibers with minimal diameter by adjusting PXDDA concentration, voltage, and flow rate. After electrospinning, PXDDA/PVA nanofibers were crosslinked using glutaraldehyde and hydrochloric acid vapor to improve their stability. Additionally, clindamycin-loaded zeolite particles at different concentrations were prepared to control drug burst release, followed by centrifugation to remove unloaded drug. These centrifuged capsules and capsules without centrifuging in different concentrations were incorporated into the polymer solutions for electrospinning. The morphology, hydrophilicity, drug release behavior, and release kinetics of the resulting nanofibers were subsequently evaluated. Also, antibacterial properties, MTT, and cell attachment of samples were investigated.

2 Experimental

2-1 Materials

Poly (xylitol-co-dodecanedioic acid) (PXDDA) polymer with high purity percentage with molecular weight 7196 g/mol, was synthesized from its monomers and PVA with molecular weight 3000-70000 was prepared from Sigma Aldrich (USA). Zeolite purchased from Tianjin Yuanli Chemical Co. Ethanol solvent was purchased from Merck company (Germany), and Phosphate buffer saline (PBS, PH= 7.4) was prepared from Roman Industrial Company (USA). Also, clindamycin drugs were purchased from Mofid Pharmaceutical Co. Deionized (DI) water was used in all experiments.

2-2 Methods

2-2-1 Encapsulation of CD into ZO particles

To construct capsules with a high drug loading, ZO particles were employed. Firstly, ZO particles were dissolved in distilled water and ultrasonically agitated for 10 min. Secondly, clindamycin drug with 2% (w/w) was loaded into ZO particles in different concentrations, including 2% (w/w) and 5% (w/w), with 2 ml of deionized water. Then, capsules were centrifuged to remove the supernatant, and the solid capsules were dried in a vacuum overnight.

2-2-2 Encapsulation efficiency

The encapsulation efficiency of clindamycin drug in ZO particles was evaluated. 5 ml of each sample, including CD/ZO particles (2/2)% w/w and (2/5)% w/w were taken and centrifuged at 8000 rpm for 15 min. After that, supernatant was taken in triplicate and absorbance values were measured using a UV-Vis spectrophotometer at 203 nm [21]. During the encapsulation process, centrifugation at 8000 rpm selectively removed unbound or weakly surface-associated clindamycin molecules. This step ensured that only the drug molecules firmly adsorbed or entrapped within the ZO particles remained in the final capsule structure. The percentage of encapsulation efficiency was assessed using Eq.(1):

$$Entrapment\ efficiency\ \% = \frac{(Amount\ of\ total\ drug - Amount\ of\ free\ drug)}{Amount\ of\ total\ drug} \times 100 \quad (1)$$

2-2-3 Electrospinning of PXDDA/PVA/capsule polymer solutions

According to a previous paper, Poly (xylitol-co-dodecanedioic acid) (PXDDA) was synthesized from Xylitol and Dodecanedioic acid monomers with a molar ratio (50:50) by polycondensation reactions. PXDDA polymer solution with concentrations of (2.9, 5, 10, 15, 17.07) % (w/w) was prepared using ethanol as solvent and stirring for 1 h. PXDDA polymer solution could not be electrospun alone; therefore, a PVA polymer solution with a concentration of 10% (w/w) in deionized water was added to the PXDDA polymer solution. To determine optimal nanofibers in morphology and the lowest diameter, the Response Surface Methodology (RSM) model was used with changing different parameters such as concentration of PXDDA polymer solution (2.9-17.07)%, voltage (12-27) kV, and flow rate (0.3-1.1) ml/h. On the other hand, the distance from the needle tip to the collector (18cm) and rpm 100 were stable. By the electrospinning method, the solvent was evaporated from the polymer jet, and nanofibers were collected on the aluminum foil to dry at room temperature. According to the RSM model, the best sample in the lowest diameter and suitable morphology includes nanofibers with a concentration of 17.07% PXDDA, PVA 10%, voltage 20 kV, and flow rate 0.75 ml/h. The scaffold prepared without a cross-linking agent is very easy to dissolve and does not have suitable mechanical structural properties. Therefore, to decrease the hydrophilicity of nanofibers and stabilize water absorption, the vapor phase crosslinking was prepared with glutaraldehyde and hydrochloric acid (HCL) in a molar ratio (9:1) in an oven at 35° C at different times. The optimal time was determined to crosslink of nanofibers that wasn't caused to disturb on scaffolds. Then, capsules including CD/ZO in different concentrations (2/2)% (w/w) and (2/5)% (w/w) with centrifugation state and without centrifugation state to compare drug release from nanofibers were loaded into PXDDA/PVA polymer solution to fabricate nanofibers by an electrospinning setup.

2-3 Characterization of ZO particles

2-3-1 Scanning electron microscopy (SEM)

The surface features and morphology of ZO particles were examined using Scanning Electron Microscopy (SEM). The particles were analyzed under an accelerating voltage range of 1 to 50 kV. Additionally, the morphology of the nanofibers was also observed using SEM. To enhance conductivity, the samples were sputter-coated with gold at an accelerating voltage of 15 kV, and images were captured at different magnifications. The average fiber diameter and its distribution were calculated based on 100 random measurements, processed using Digimizer software.

2-3-2 Dynamic light scattering (DLS) of ZO particles

The particle diameter can be determined by dynamic light scattering (DLS) with the aid of Brownian movement and its light scattering properties. The analysis of light scattered from the interaction of light and matter provides insights into the physical properties of the sample. The particle size distribution and intensity of ZO particles were determined using DLS. Specific conditions, such as a temperature of 25 °C and a dispersion angle of 90° C were set during the analysis.

2-3-3 X-ray Diffraction (XRD) of ZO particles

The Rigaku Benchtop Mini-ex-device, using Cu-Kα as a radiation source (1.5406 Å) at 10 mA with 40 kV in the 20°–80° angle range, verified the purity of the crystal structure and phase formation in the ZO particles through XRD studies.

2-3-4 Fourier transform infrared spectroscopy (FTIR)

The powder of ZO particles, PXDDA/PVA nanofibers, and PXDDA/PVA/Capsules without crosslinking and with crosslinking were investigated using FTIR to visualize the functional groups present in the nanofibers. Sample wavelengths were captured with a scanning resolution at the ambient temperature of 16 °C in the medium infrared range from 4000 cm^{-1} to 400 cm^{-1}.

2-4 Modeling and optimization of PXDDA/PVA nanofibers

2-4-1 Response Surface Methodology (RSM)

The Response Surface Methodology (RSM) is a statistical technique used to model and quantify the relationships between one or more measured responses and key input factors. The goal is to identify an optimal point within the design space. Additionally, RSM allows for the estimation of the coefficients of the mathematical model, with accuracy assessed based on experimental data [22]. In this study, RSM was applied to evaluate the impact of three independent variables: polymer solution (X_1), applied voltage (X_2), and flow rate (X_3) on the nanofiber diameter (Y). The Box-Behnken design, a type of response surface design, was used, and since three factors were involved, a quadratic model was deemed appropriate. The experimental parameters for each factor are outlined in Table 1. Replicating the design points helps estimate the pure error (Ɛ) in the design. The statistical software Design-Expert was employed for regression analysis of the experimental data and to generate the response surface plots [22]. Affecting the diameter of PXDDA/PVA nanofibers represented by Y (Equation 2, 3). f and ε are the activation function and error parameter, respectively.

$$Y = f(X_1, X_2, X_3) \pm \mathcal{E} \quad (2)$$

$$f = a_0 + \sum_{1}^{3} a_i x_i + \sum_{1}^{3}\sum_{1}^{3} a_{ij} x_i x_j + \sum_{1}^{3} a_{ii} x_i^2 \quad (3)$$

Table 1 Parameters in various levels in RSM models

Factor	Name	PXDDA/PVA Levels		
		-1	0	+1
X_1	Concentration (%)	5	10	15
X_2	Voltage (kV)	15	20	25
X_3	Flow rate (ml/h)	0.5	0.7	1

2-4-2 Hydrophilicity of PXDDA/PVA nanofibers

The contact angles were measured using the drop test method by an optical video contact angle instrument before and after crosslinking. Different types of nanofibers, including PXDDA/PVA, PXDDA/PVA/capsule (2%, 5%) were prepared. A droplet of distilled water was deposited on the nanofibers. The contact angle was measured on 3 different points, and the average values and standard deviation were calculated using Digimizer software.

2-4-3 In vitro capsule release

To assess the release of the capsule, nanofiber samples (2 × 2 cm²) were immersed in 8 mL of phosphate-buffered saline (PBS, pH 7.4) as the release medium for the in vitro drug release study. The samples were then placed in a shaking incubator at 37°C. At predetermined time intervals, 3 mL of the release medium was removed and replaced with an equal volume of fresh PBS. The absorbance of the released capsule in the PBS was measured using a UV-visible spectrophotometer (Shimadzu, Japan), with the characteristic peak of the capsule appearing at a maximum wavelength of 203 nm. The UV absorbance calibration curve was plotted against drug concentration, based on the Beer-Lambert equation (Eq. (4)), with an R-value of approximately 0.9416 (Figure 1). At each time point, the absorbance was recorded and the corresponding concentration of the released capsule was calculated using a standard curve (absorbance vs. capsule concentration in PBS). The cumulative release of the capsule from the samples was monitored over 48 hours, and the percentage of cumulative release (Er) was calculated as described in Eq. (5):

$$A = \varepsilon l c \quad (4)$$

$$E_r(\%) = \frac{V_0 \times C_n + V_r \times \sum_1^{n-1} C_i}{m_{total}} \times 100 \quad (5)$$

Where mtotal denotes the capsule content encapsulated in the nanofiber mats, V0 and Vr are the volume of the release media and the replaced media, respectively, and Cn is the capsule concentration in the sample [23].

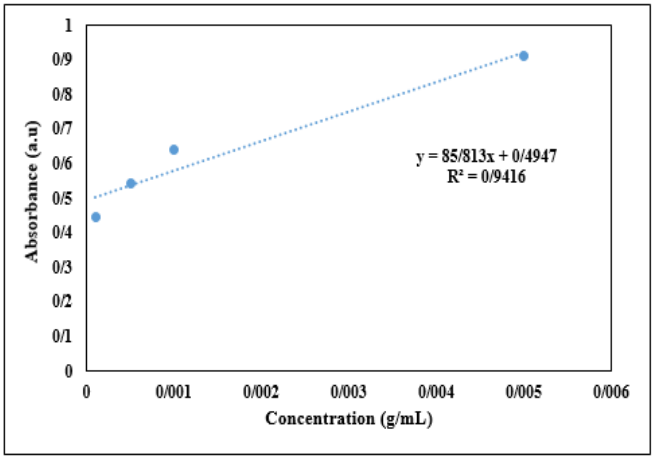

Figure 1 Standard curve of CD

2-4-4 Kinetics of capsule ZO/Drug release

The cumulative release data were fitted with the following models to realize the release mechanism of the capsule:

- Zero- order kinetics model:

$$M_0 - M_t = K_0 t \quad (6)$$

- First- order kinetics model:

$$\log(100 - Mt) = \log 100 - \frac{K_1}{2.303} t \quad (7)$$

- Higuchi kinetics model:

$$M_t = K_{HC} (t^{1/2}) \quad (8)$$

In this context, Mt represents the drug concentration released at time t, while M0 refers to the initial drug concentration in the solution. The constants k_0, k_1, and k_{HC} correspond to the drug release rate for zero-order, first-order, and Higuchi kinetics models, respectively.

- Korsmeyer- Peppas model:

$$\frac{M_t}{M_\infty} = K_{kp} . t_n \quad (9)$$

That M_t/M_∞ is the released drug fraction at the time of t, k_{kp} denotes the constant of release rate, and n denotes the release exponent [23].

2-4-5 Antibacterial of nanofibers

The antibacterial activity of the crosslinked PXDDA/PVA nanofibers containing CD/ZO at concentrations of (2/2)% and (2/5)%, evaluated both with and without capsule centrifugation, was tested against S. aureus and E. coli. Square nanofiber specimens (2 × 2 cm²) were fabricated and subjected to UV sterilization for 2 hours. Following sterilization, the samples were placed in a bacterial culture medium and incubated at 37 °C for 24 hours. The antimicrobial efficacy was determined by measuring the inhibition zones formed around each nanofiber sample.

2-4-6 Cell viability of nanofibers

The cytocompatibility of the fabricated nanofibers was examined by determining the viability of mesenchymal stem cells (MSCs) through the MTT colorimetric assay. MSCs were cultured in Dulbecco's Modified Eagle Medium (DMEM) supplemented with 10% fetal bovine serum and maintained at 37 °C in an incubator containing 5% CO_2. Before cell exposure, the nanofiber samples were disinfected under UV irradiation for 2 hours, rinsed in PBS for 30 minutes, and subsequently kept in fresh medium overnight. Each sterilized nanofiber was then transferred to a 48-well plate seeded with MSCs (1 × 10⁴ cells in 500 µL of medium) and allowed to interact with the cells for 24 hours. After incubation, the wells were gently washed with PBS, and 100 µL of an MTT working solution (0.5 mg/mL in PBS) was added. The plates were returned to the incubator at 37 °C for 30 minutes to enable the conversion of MTT into insoluble purple formazan by metabolically active cells. The appearance of these crystals served as an indicator of cell viability in contact with the nanofiber samples. After incubation, the medium was discarded, and 200 µL of dimethyl sulfoxide was added to dissolve the formazan crystals. The optical density was measured using an ELISA reader at 570 nm, and cell viability (%) was calculated using Eq. (10) [23].

$$\text{Cell viability (\%)} = \left(\frac{Average\ optical\ density\ of\ sample}{Average\ optical\ density\ of\ control}\right) \times 100 \quad (9)$$

Measurements were taken over 1, 2, and 3 days.

2-4-7 Cell culture of nanofibers

For assessing cellular adhesion and proliferation, nanofiber samples (0.5 mm²) were first disinfected using UV exposure for 2 hours. Mesenchymal stem cells (MSCs) were then seeded onto the nanofiber surfaces at a density of 2,000 cells per sample in 96-well plates, with 200 µL of culture medium added to each well. The cultures were maintained at 37 °C, and cell behavior was monitored over incubation periods of 1, 3, and 5 days. At the end of the 5 days, the scaffolds were carefully taken out of the wells, and the extent of cell attachment and spreading on the fibers was examined using scanning electron microscopy (SEM).

2-5 Statistical analysis

All experiments were implemented in triplicate and the average ± standard deviation (SD) of the mean was used for the presentation of the results. Statistically significant differences between groups were analyzed using one-way ANOVA and Student's t-test. A value of $p < 0.05$ was assumed significant.

3 Results and discussions

3-1 Characterization of ZO particles

3-1-1 Scanning electron microscopy (SEM)

Zeolite particles have a cylindrical shape with a smaller particle size (1.5- 2 µm) as demonstrated in Figure 2 with different magnifications. Shiying Li et al., showed that zeolite particles are cylindrical particles with 0.9-1.2 µm [24].

3-1-2 Dynamic light scattering (DLS) of ZO particles

The size of particles has been measured using the DLS technique. The results obtained for the ZO particles are demonstrated in Figure 2 according to the SBL algorithm. In Figure 3, analysis of the obtained results shows that approximately 90% of particles have 1500- 2000 nm. Also, Mohana Haghbin et al. exhibited that the size of the pure ZO without loading drug was 2959 nm [25].

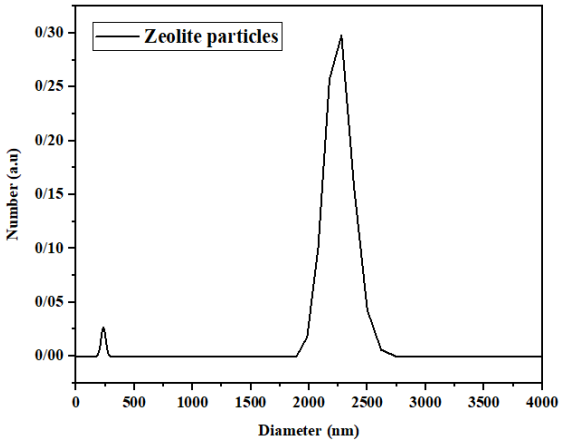

Figure 2 The size of ZO particles with SBL algorithm by DLS technique

3-1-3 Fourier transform infrared spectroscopy (FTIR)

FTIR analysis was utilized to determine functional groups that exist in ZO particles (Figure 4). The peaks of ZO at 3410, 1631, 1226, 1097, 795, 545 cm^{-1} correspond to the bending mode of water (O-H), asymmetric stretching vibration of Si-Al-O group, asymmetric stretching vibration of Si-O-Si, and Si-O-Al were attributed to the asymmetric stretching modes and symmetric stretching vibration of Si-Al-O. The functional groups of the capsule, including encapsulation of the clindamycin drug into the ZO particles, did not show considerable changes in peaks. Loading the drug into particles was intended to enhance absorbance peaks in comparison to functional groups in ZO particles. Sanam Mohandesnezhad et al could obtain similar results about functional groups in ZO particles [26].

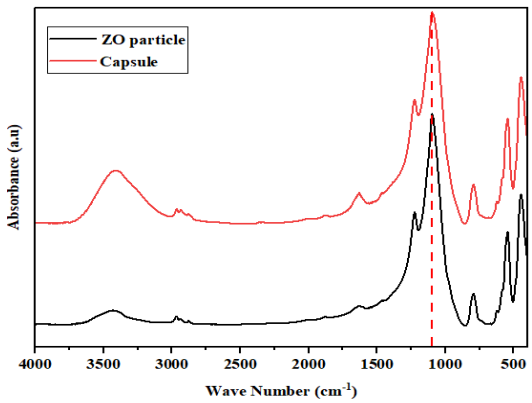

Figure 3 FTIR of ZO particles

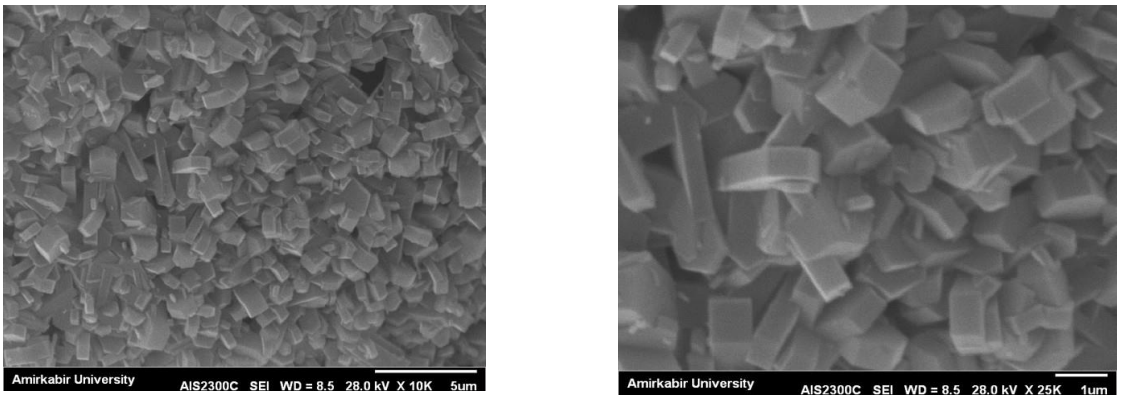

Figure 4 SEM images of zeolite particles in different magnifications

3-1-4 X-ray of ZO particles

The XRD pattern of the synthesized ZO particles is presented in Figure 5. Distinct diffraction peaks were observed at 2θ = 7.67°, 9.91°, 17.68°, and 24.29°, corresponding to the (538), (609), (855), and (1062) crystal planes, respectively. These peaks align well with characteristic reflections reported for zeolite structures in previous studies. For instance, Guo et al. [27] and Kiradzhiyska et al. [28] similarly reported diffraction peaks in the 2θ range of 7–30°, confirming the presence of well-defined crystalline zeolite frameworks. The agreement between our obtained peaks and those in the literature verifies the crystalline nature of the synthesized ZO particles and confirms the successful formation of the zeolite structure.

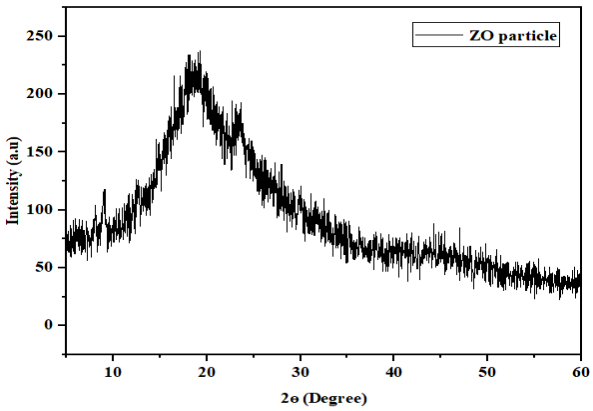

Figure 5 XRD patterns of ZO particles

3-1-5 Encapsulation efficiency of drug into ZO

The samples, including CD into ZO particles, exhibited high encapsulation efficiencies, ranging from approximately 90% to 97% that are shown in Figure 6. Among them, the formulation without centrifugation (2/5)% showed the highest efficiency (97%), indicating that only a very small fraction of clindamycin hydrochloride was released during the initial 24 h. The samples prepared under centrifugation conditions also maintained high EE values (92-90)%, confirming that the ZO effectively entrapped the drug. Overall, the minimal early drug loss and consistently high EE values across all formulations demonstrate the strong loading capability and stability of the developed ZO particles.

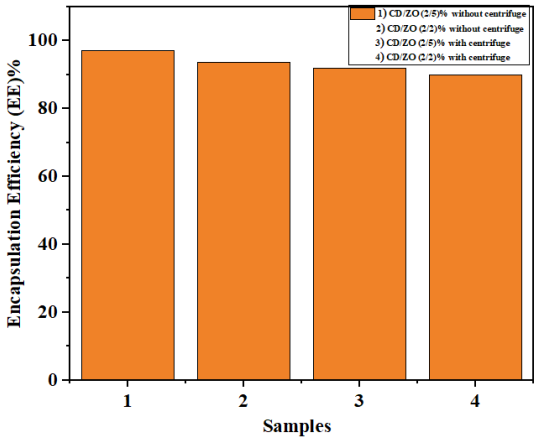

Figure 6 Encapsulation Efficiency of samples, including 1) CD/ZO (2/5)% without centrifuge, 2) CD/ZO (2/2)% without centrifuge, 3) CD/ZO (2/5)% with centrifuge, and 4) CD/ZO (2/2)% with centrifuge during 24 h

3-1-6 Drug release of CD from the capsule

The results show the cumulative release behaviour of CD from CD/ZO capsules with two different CD/ZO ratios (2/5)% and (2/2)%, comparing samples prepared with centrifugation and without centrifugation over a 2-hour release period (Figure 7). Across all samples, the release profile follows a nearly linear trend, indicating a predominantly diffusion-controlled release mechanism during the early phase. However, significant differences in release rates are observed depending on both the CD/ZO ratio and the application of centrifugation. At 0.5 hours, the non-centrifuged samples show noticeably higher release values compared to their centrifuged counterparts. For example, the CD/ZO (2/5)% without centrifugation exhibits the highest early release, while the CD/ZO (2/5)% with centrifugation demonstrates the lowest release at this time point. This suggests that the absence of centrifugation may lead to a looser or less compact microstructure, facilitating faster initial diffusion of CD. At 1 hour, this trend remains consistent. The non-centrifuged samples (both 2/5% and 2/2%) maintain higher cumulative release, with the (2/2)% non-centrifuged formulation showing the highest release among all samples. In contrast, centrifuged capsules release CD more slowly, likely due to improved structural uniformity and tighter compaction resulting from centrifugal processing, which can restrict drug mobility. By 2 hours, the differences between samples become even more pronounced. The CD/ZO (2/2)% without centrifugation reaches approximately 65% cumulative release, the highest among all groups. Conversely, the centrifuged (2/5)% sample exhibits the lowest release (~33%). The (2/2)% centrifuged sample also shows moderate release (~45%), indicating that the CD/ZO ratio affects release behaviour in addition to centrifugation. Lower ZO content (2/2)% appears to facilitate a faster drug release compared to higher ZO content (2/5)%, likely due to reduced structural density or decreased barrier properties. Overall, the results indicate that centrifugation significantly slows drug release, producing more controlled and sustained release profiles by increasing capsule compactness and structural integrity. In contrast, non-centrifuged samples release CD more rapidly, particularly in samples with lower ZO content. These findings demonstrate that both the processing method (centrifugation) and compositional ratio (CD/ZO) play crucial roles in tuning the release kinetics of CD-loaded capsules.

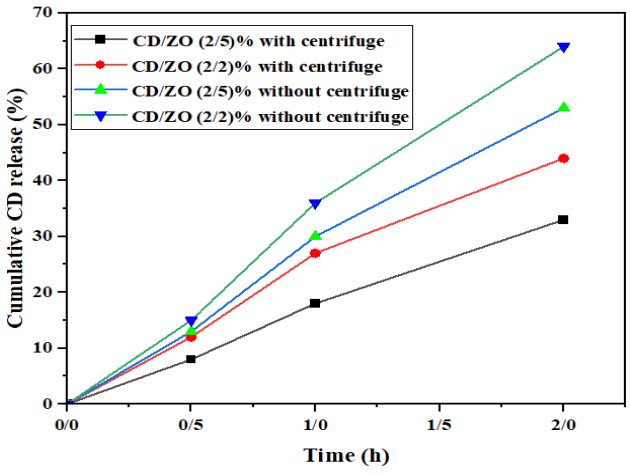

Figure 7 Drug release from ZO particles during 2 h

3-2 Characterization of PXDDA/PVA nanofibers

3-2-1 RSM model

To determine optimal nanofibers with the smallest diameter and highest quality (low beads), the experimental design included 15 experimental tests (Table 2). According to Table 2, three factors, including concentration of PXDDA polymer solution, voltage, and flow rate, were changed to determine the best sample in the lowest diameter and the best morphology. The results showed that sample 6, with a diameter of 395± 76 nm, was the best sample in terms of diameter and morphology. Standard analysis of variance (ANOVA) was performed to analyze the response surface. Table 3 exhibits the corresponding RSM responses (fiber diameter and quality factor) to affect different parameters on the diameter and morphology of nanofibers. Concentration of PXDDA polymer solution with the lowest Pvalue had the most effective on the diameter of nanofibers, as shown in Figure 8. However, increasing of polymer solution concentration to the optimal point caused to augment diameter of the nanofibers due to an increase in the viscosity of the polymer solution. Increasing the PXDDA polymer concentration was triggered to decrease the diameter of nanofibers. Because the solvent of this polymer was ethanol, and this solvent in high concentration in the polymer solution could cause a decrease in the viscosity of the polymer solution. On the other hand, the voltage parameter with Pvalue= 0.0025 had an effective factor on the diameter of nanofibers. However, the increase in voltage was triggered to reduce the diameter of nanofibers due to the more effective polymer solution concentration on the polymer jet to produce nanofibers on the collector. These results are demonstrated in a 3D surface (Figure 9).

According to this diagram, the flow rate did not have a significant effect on the diameter of the nanofiber. Also, the ANOVA results exhibited that the flow rate factor had P>0.05. According to the RSM model that could predict the best sample in diameter of nanofibers, Figure 10 shows that the regression diagram of the prediction model vs actual model is so similar that are demonstrated in the code equation and actual equation.

Table 2 Experimental design expert to determine the optimal sample in diameter with changing various factors

	Factor 1	Factor 2	Factor 3	Response 1
Run	A:Concentration	B:Voltage	C:Flow rate	Diameter
	%	kV	ml/h	nm
1	10	20	0.75	932± 172
2	10	20	0.39	931±181
3	2.9	20	0.75	628 ± 138
4	10	12.9	0.75	811±145
5	10	20	0.75	900 ±156
6	17.07	20	0.75	395± 76*
7	15	15	1	1066 ±160
8	10	20	1.1	886 ±155
9	10	20	0.75	895± 102
10	10	20	0.75	921 ± 125
11	10	20	0.75	905 ± 178
12	5	25	1	483± 96
13	15	25	0.5	1222 ± 235
14	5	15	0.5	477 ±106
15	10	27.07	0.75	959 ± 175

*Optimal sample

Table 3 Statistical analysis with ANOVA table

Source	Sum of Squares	df	Mean Square	F-value	p-value	
Model	7.471E+05	10	74712.64	313.52	< 0.0001	significant
A-Concentration	27144.50	1	27144.50	113.91	0.0004	
B-Voltage	10952.00	1	10952.00	45.96	0.0025	
C-Flow rate	1012.50	1	1012.50	4.25	0.1083	
AB	932.26	1	932.26	3.91	0.1191	
AC	279.70	1	279.70	1.17	0.3396	
BC	3.434E+05	1	3.434E+05	1441.12	< 0.0001	
A^2	2.275E+05	1	2.275E+05	954.86	< 0.0001	
B^2	936.23	1	936.23	3.93	0.1185	
C^2	6.30	1	6.30	0.0264	0.8787	
ABC	19524.50	1	19524.50	81.93	0.0008	
Pure Error	953.20	4	238.30			
Core Total	7.481E+05	14				

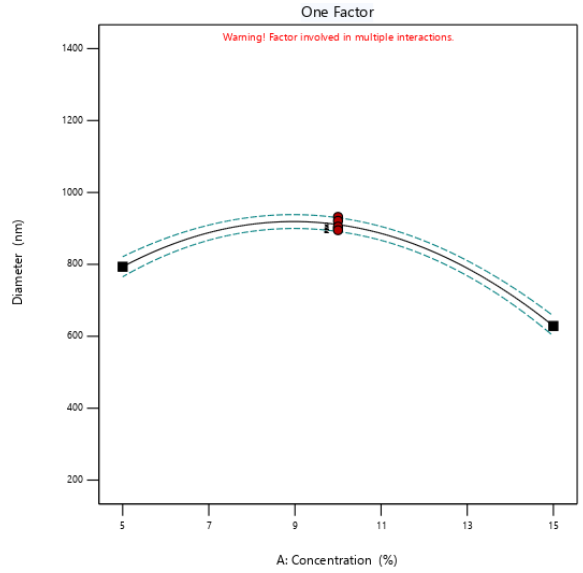

(a)

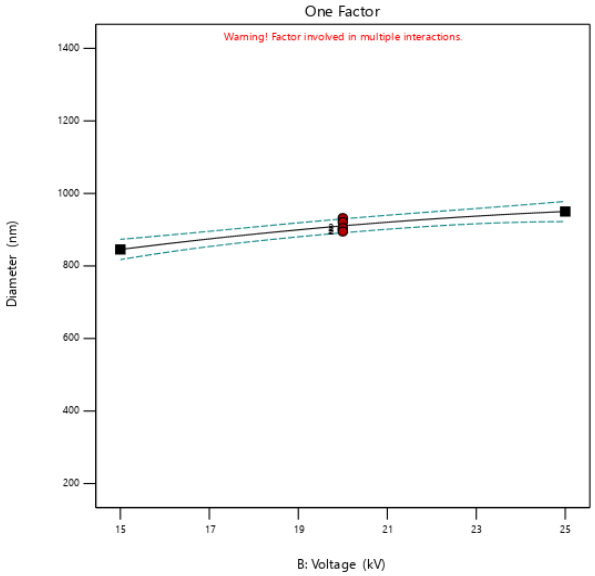

(b)

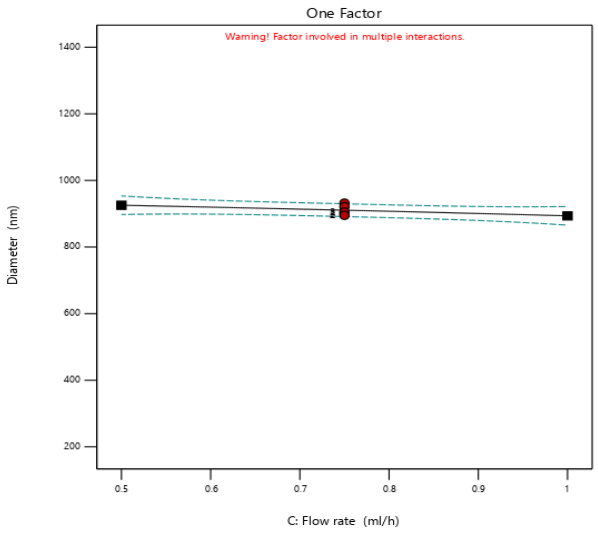

(c)

Figure 8 One factor diagram of affecting different parameters including a) concentration of PXDDA polymer solution, b) Voltage, and c) flow rate on the diameter of nanofibers

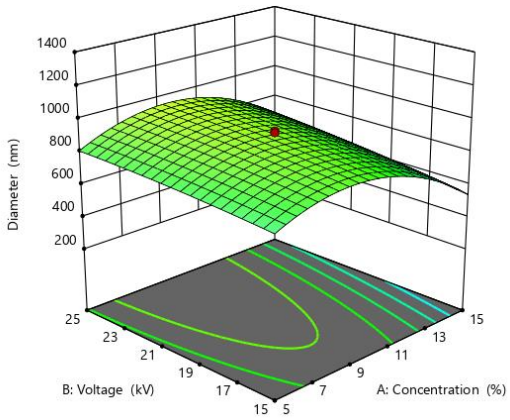

(a)

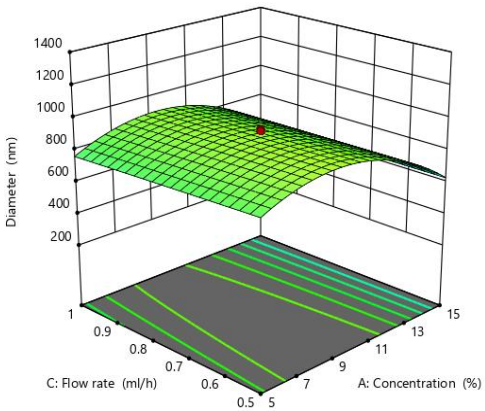

(b)

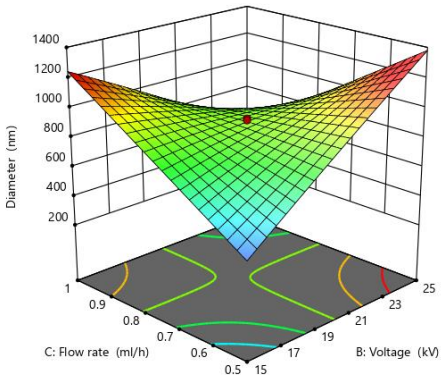

(c)

Figure 9 3D surface of synergistic affecting parameters on the diameter of nanofibers

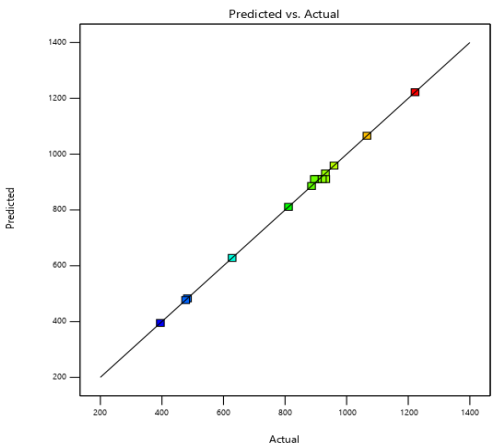

Figure 10 The regression diagram of prediction vs. actual model

Code Equation:

$$\text{Diameter} = 910.060 - 82.38\,A + 52.38\,B - 15.91C + 21.59\,AB + 11.83\,AC - 414.38\,BC - 199.55\,A^2 - 12.80\,B^2 - 1.05\,C^2 - 114.80\,ABC \quad (9)$$

Actual Equation:

$$\text{Diameter} = -2072.32711 - 156.72321\,A + 133.17591\,B + 2823.40022\,C + 14.63960\,AB + 376.82072\,BC - 147.82235\,AC - 7.98200\,A^2 - 0.512000\,B^2 - 16.80000\,C^2 - 18.36800\,ABC \quad (10)$$

3-3 Characterization of PXDDA/PVA nanofibers

3-3-1 Morphology of PXDDA/PVA nanofibers

Figure 11 displays the morphological features and diameter distribution of the fabricated composite nanofibers. Randomly oriented, bead-free, and smooth surfaces with an average diameter of 395 ±76 nm were observed for PXDDA/PVA nanofibers. In contrast, the incorporation of capsules into polymer solutions to fabricate nanofibers was triggered a considerable change in the fiber morphology, signifying the uniform capsule distribution in the polymer solution. Therefore, adding CD/ZO in concentrations of (2/2)% and (2/5)% (w/w) into polymer solutions exhibited slightly rough and irregular surfaces along with enhanced mean diameters to 545 ±110 nm and 588 ±149 nm, respectively. The main reason was due to increase viscosity of the polymeric solution, a higher charge density is created on the polymer jet, leading to the fiber diameter and the formation of a rough and irregular fiber surface. By trapping the capsule in polymer solutions, the diameter of the nanofibers was enhanced. So, Fatemeh Haghdoost et al exhibit loading zeolite into polyethersulfone/polyvinyl pyrrolidone polymer solution to fabricate nanofibers to noticeably increase the diameter of nanofibers [20].

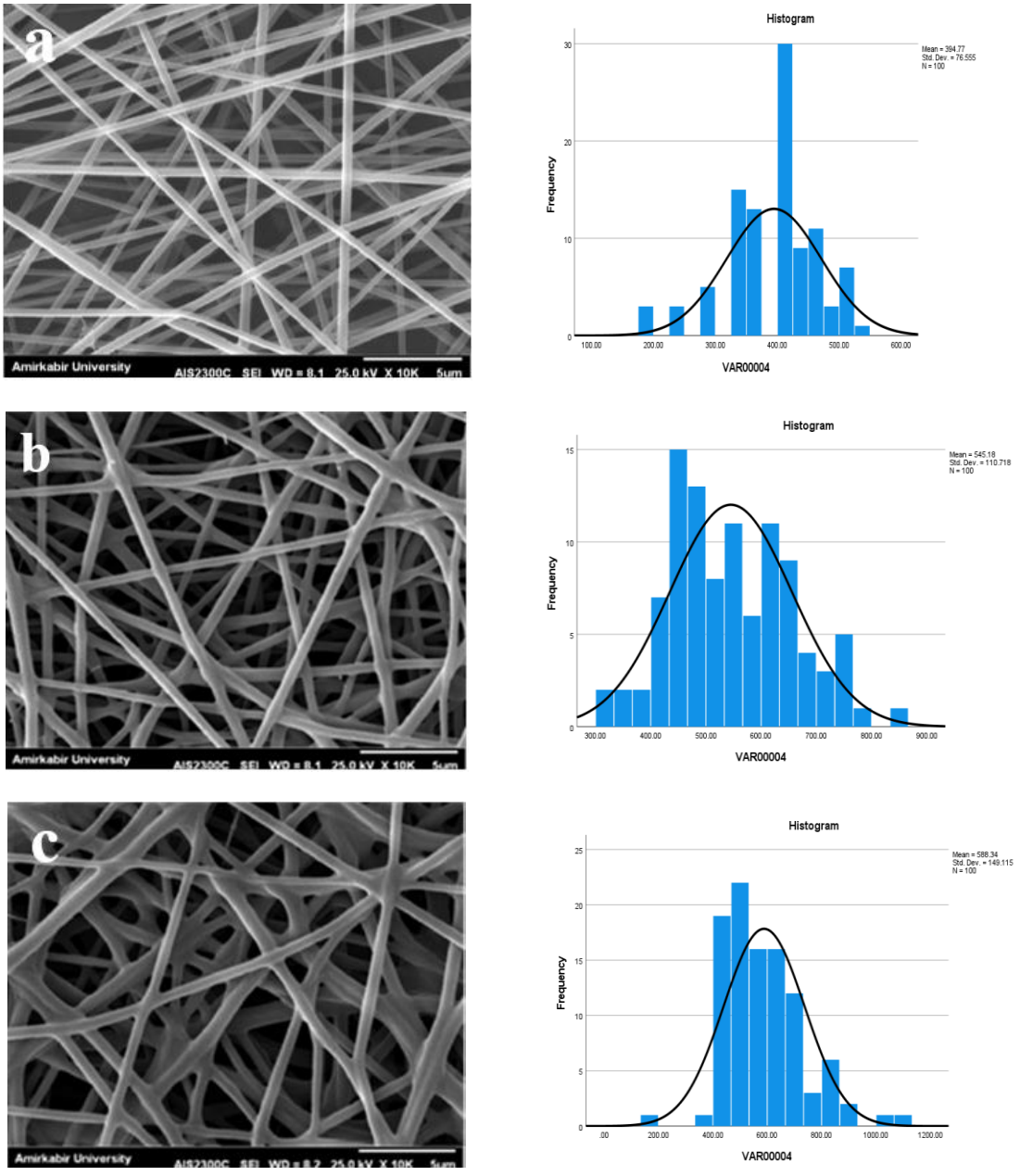

Figure 11 SEM images of nanofibers a) PXDDA/PVA, b) PXDDA/PVA/CD/ZO (2/2) %, and c) PXDDA/PVA/CD/ZO (2/5) %

3-3-2 Crosslinking of PXDDA/PVA/Capsule nanofibers

PXDDA and PVA nanofibers are hydrophilic polymers that adsorb water molecules. Therefore, to enhance the water stability on the surface of nanofibers was used at different times. Crosslinking of nanofibers helps to control drug release from them for the treatment of damaged tissues. Figure 12 shows the SEM micrographs and diameter distribution of PXDDA/PVA nanofibers with loading capsules into them at different times. The results demonstrated that PXDDA/PVA nanofibers were crosslinked from 1.5 hours to 4.5 hours in an oven at 35°C as exhibited in Figure ١٢a-١٢d. However, loading the capsule into nanofibers was triggered to disturb the nanofibers in 4.5 hours; therefore, the best time to crosslink PXDDA/PVA/Capsule was 3.5 hours, as shown in Figure ١٢g. After crosslinking by immersing samples in distilled water, it helped to decrease toxicity due to glutaraldehyde vapour.

3-3-3 Hydrophilicity of PXDDA/PVA/Capsule nanofibers

Surface hydrophilicity of membranes plays an important role in cell viability and treating damaged tissues. Generally, the hydrophilicity of membranes can be assessed by measuring the contact angle of water on the membrane. With increasing hydrophilicity of nanofibers, the water droplets permeate with low pressure into nanofibers to create a low contact angle compared to the hydrophobic properties of nanofibers. Surface chemistry, including the contact angle and wettability of solid nanofibers, has been widely studied. Figure 13 shows the hydrophilicity of PXDDA/PVA nanofibers that were crosslinked under glutaraldehyde vapour for 3.5 hours. These polymers are hydrophilic with a contact angle 34 ±7 ° (Figure 13a). Crosslinking of PXDDA/PVA nanofibers could prevent dissolving nanofibers into water; however, their wettability was considerable. Loading capsule (CD/ZO particles) without centrifuging in different concentrations into polymer solutions caused an increase in contact angle due to the creation of roughness on the surface of nanofibers and attachment of hydroxyl groups of the capsule with hydrophilic groups of PXDDA/PVA polymers. Therefore, the low group factors can attach to the hydroxyl groups of water to decrease the contact angle. However, adding a capsule without centrifuging into polymer solutions results in the drug being distributed into ZO particles and out of ZO particles, and is triggered to increase the hydrophilicity of nanofibers in comparison to a capsule with centrifuged into polymer solutions. Because the centrifuging stage includes the drug in ZO particles, and there is no drug in the polymer solutions. According to Figure 13b, the contact angle of PXDDA/PVA nanofibers with loading (2/2)% (w/w) CD/ZO particles without centrifuging was 39± 3°, which was higher than the sample without a capsule, because of increasing surface roughness of nanofibers with adding a capsule into polymer solutions to fabricate nanofibers. Another reason is related to attaching hydroxyl groups of the capsule with hydrophilic groups of PXDDA/PVA polymers; therefore, the hydroxyl groups of water face with lower hydrophilic groups of polymers in comparison to nanofibers without a capsule.

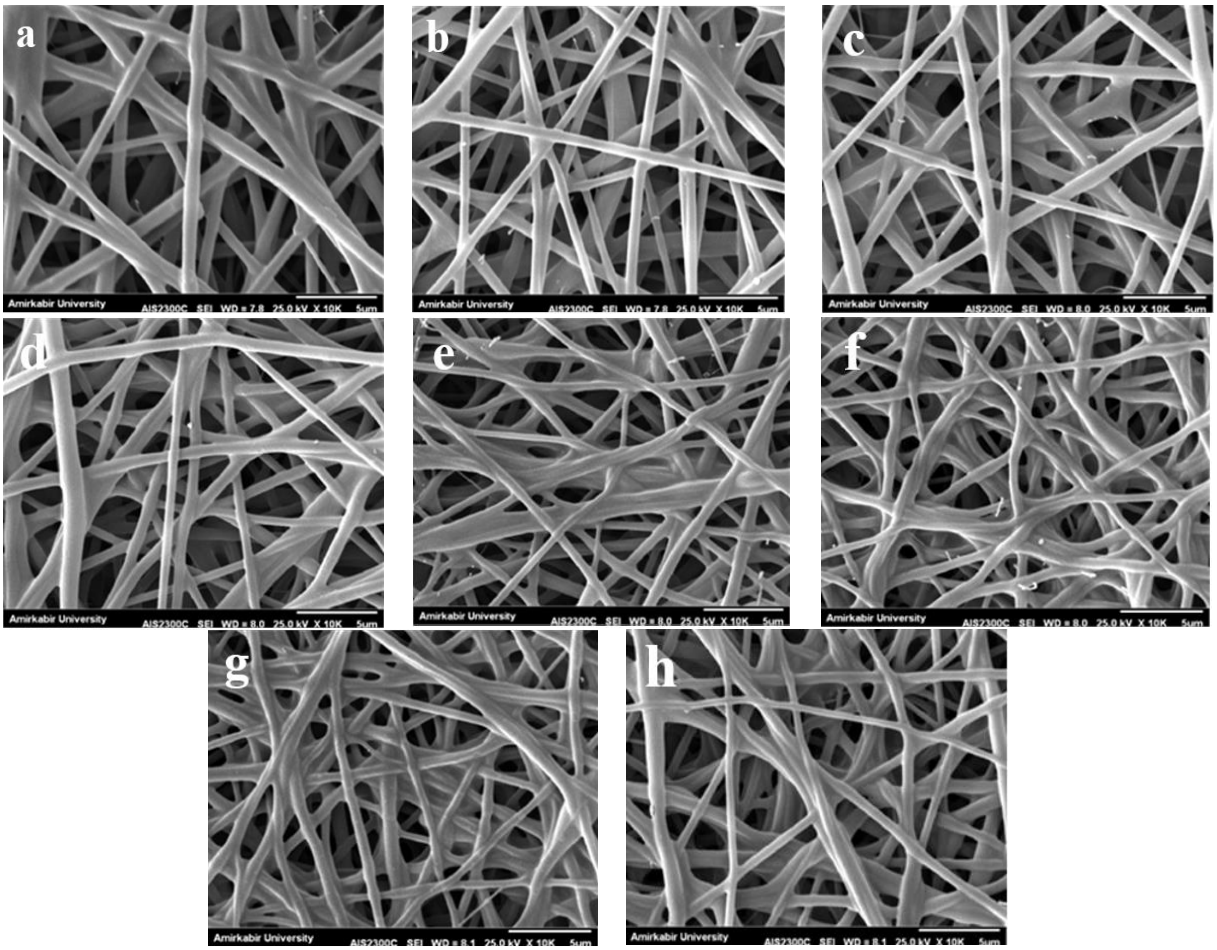

Figure 12 SEM images of nanofibers crosslinking in different time including crosslinking of PXDDA/PVA nanofibers in a) 1.5h, b) 2.5 h, c) 3.5 h, d) 4.5 h, and crosslinking of PXDDA/PVA/Capsule in e) 1.5 h, f) 2.5 h, g) 3.5 h, and h) 4.5 h

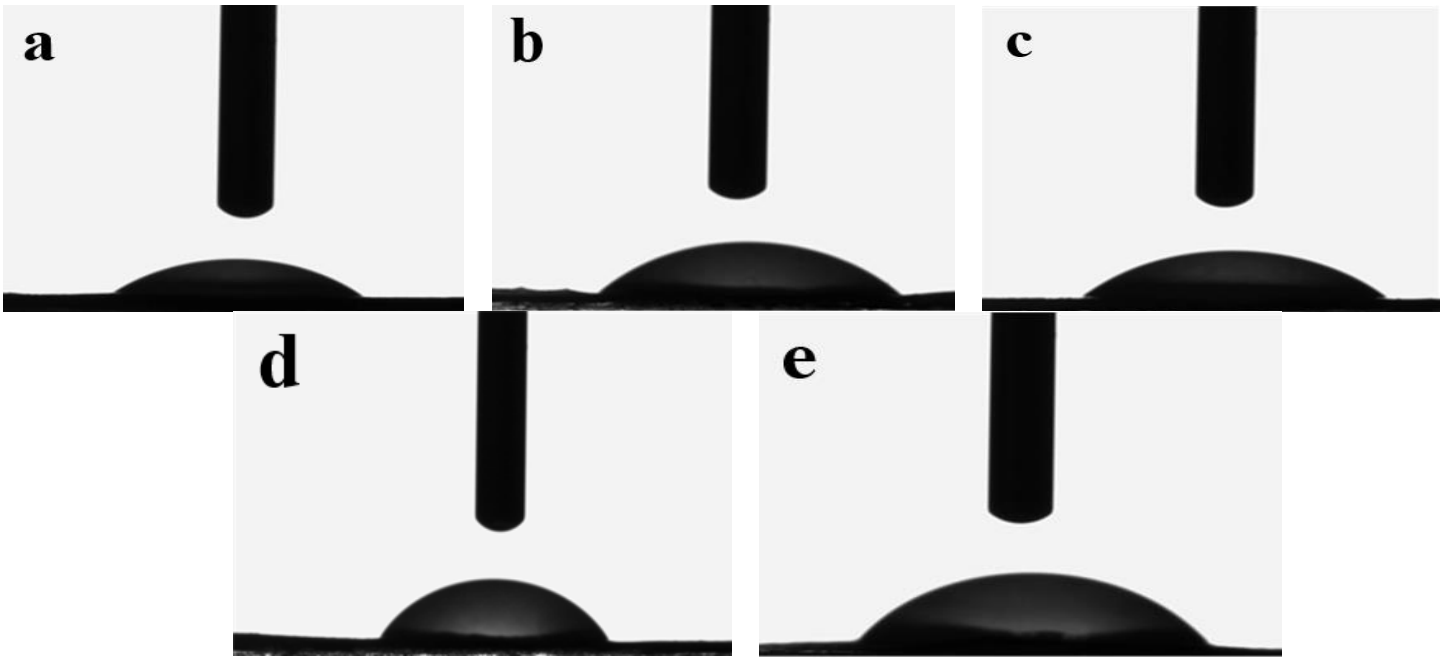

Figure 13Contact angle of nanofibers with crosslinking a) PXDDA/PVA, b) PXDDA/PVA/CD/ZO (2/2)% (w/w) without centrifuge, c) PXDDA/PVA/CD/ZO (2/5)% (w/w) without centrifuge, d) PXDDA/PVA/CO/ZO (2/2)% (w/w) with centrifuge, and e) PXDDA/PVA/CO/ZO (2/5)% (w/w) with centrifuge

However, increasing the concentration of the capsule of CD/ZO particles to (2/5)% helped to decrease the contact angle to about 36 ±0.03° (Figure 13c) due to the hydroxyl groups absorbed on the surface of the membrane. Moreover, Figure 13d shows that loading capsule (CD/ZO particles) in (2/2)% concentration with centrifuging into polymer solutions increased the contact angle to 56 ±11° in comparison to the capsule without centrifuging. Because centrifuging of the capsule was performed to reduce free drug concentration in the polymer solution and increase the contact angle of the nanofibers. Furthermore, adding a concentration of CD/ZO particles with centrifuging to (2/5)% into polymer solutions reduces the contact angle to 52± 3.9° in comparison to loading (2/2)% capsule with centrifuging into polymer solutions. Also, Addie Bahi et al studied the hydrophilicity of lignin membrane with the incorporation of ZO nanoparticles into the membrane. The results showed that loading ZO nanoparticles can be attributed to the excellent hydrophilicity of the membrane due to hydroxyl groups in the structure of ZO nanoparticles that absorb on the surface of the membrane [29].

3-3-4 FTIR of PXDDA/PVA nanofibers

FTIR analysis of the PXDDA/PVA nanofibers showed a broad O–H stretching band (≈3200–3550 cm^{-1}) indicative of extensive hydrogen bonding, strong C–H stretches near 2900 cm^{-1}, a clear ester C=O band at ≈1700–1750 cm^{-1} confirming the presence of PXDDA, and intense C–O/C–O–C absorptions in the 1250–1050 cm^{-1} region; the spectral features are consistent with intimate PVA–PXDDA interaction and are compatible with acetal-type changes expected after glutaraldehyde vapor crosslinking. Incorporation of the capsule (CD/ZO) into nanofibers caused the overlap peaks of PXDDA/PVA nanofibers (Figure 14).

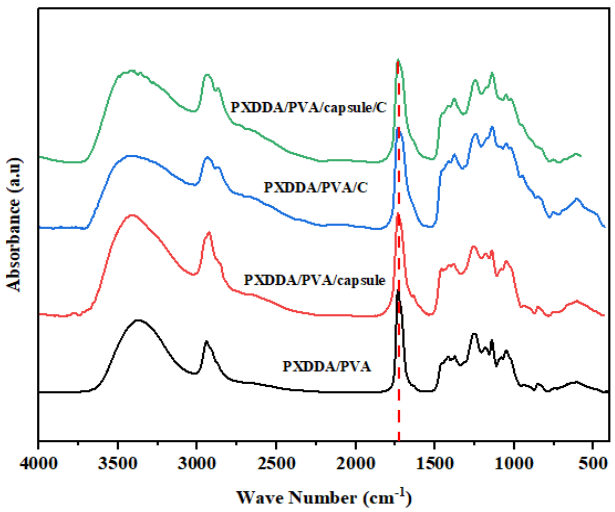

Figure 14 The functional groups of PXDDA/PVA, PXDDA/PVA/Capsule, PXDDA/PVA/C, and PXDDA/PVA/Capsule/C

3-3-5 In vitro drug release from PXDDA/PVA/Capsule nanofibers

The drug-release behavior of the crosslinked PXDDA/PVA nanofibers containing CD/ZO capsules is presented in Figure 15. A clear difference was observed between centrifuged and non-centrifuged capsules. Nanofibers containing non-centrifuged capsules exhibited a pronounced burst release during the first hours, which can be attributed to the presence of freely dispersed clindamycin molecules that were not fully loaded into the ZO structure. These unbound molecules rapidly diffused into the release medium, resulting in an early spike followed by a sharp decline in release over time. In contrast, nanofibers containing centrifuged capsules demonstrated significantly reduced burst release and a sustained release profile over 48 h. Centrifugation effectively removed unbound drug, leaving

only drug molecules that were either electrostatically adsorbed onto the negatively charged zeolite framework or physically entrapped within its micro- and–mesoporous channels. As a result, drug diffusion occurred gradually through the ZO network and crosslinked nanofiber matrix, leading to controlled and prolonged release. The concentration of ZO also influenced the release rate. Samples containing 2% drug in 2% ZO particles released a larger fraction of drug, whereas increasing ZO content to 5% led to lower cumulative release due to the higher adsorption capacity and stronger drug–carrier interactions, which retard diffusion.

Centrifugation played a critical role in minimizing the burst release of clindamycin from the nanofibers. Capsules that were not centrifuged contained a significant amount of free, non-entrapped drug dispersed in the polymer solution. This unbound drug rapidly diffused into the release medium during the first hours, resulting in a pronounced burst release. In contrast, centrifugation removed the free drug present in the supernatant, leaving behind only drug molecules that were either strongly adsorbed onto the negatively charged zeolite framework or physically entrapped within its micro–mesoporous channels. Because these interactions require diffusion through the zeolite structure before release, the initial burst was significantly reduced, and a sustained Higuchi-type release profile was achieved. This confirms that centrifugation enhances loading stability and regulates drug release by eliminating weakly associated drug fractions.

3-3-6 Kinetic of capsule release from PXDDA/PVA nanofibers

Several models were used to investigate the capsule release mechanism. Moreover, to understand the diffusion mechanism type, the Korsmeyer-Peppas kinetic model can be applied. In this model, the drug release mechanism is described by the value of n (in Eq. 8). In the case of n ≤0.45, the drug release mechanism I based on Fickian diffusion, and when 0.45 <n< 1, the drug release conforms to non-Fickian transport. If n = 1, the drug release is according to zero-order kinetics or Case-II transport. In the case of n > 1, the drug release mechanism follows super Case-II transport [23]. As shown in Table 4, the highest correlation coefficients (R^2 > 0.98 for most samples) were obtained for the Higuchi model, indicating that clindamycin release from the nanofibers is predominantly governed by diffusion through a porous matrix. Furthermore, analysis of the Korsmeyer–Peppas model showed that all samples exhibited n values < 0.45, confirming a Fickian diffusion mechanism. This behavior is consistent with the presence of a crosslinked hydrophilic network, the microporous structure of ZO particles, and the concentration gradient between the nanofiber mat and the release medium. These factors collectively regulate the diffusion pathway and distance, supporting the sustained release observed in centrifuged samples. Overall, the kinetic analysis demonstrates that the release of clindamycin from PXDDA/PVA/CD-ZO nanofibers is diffusion-controlled and significantly improved by the centrifugation step, which removes weakly bound drug fractions.

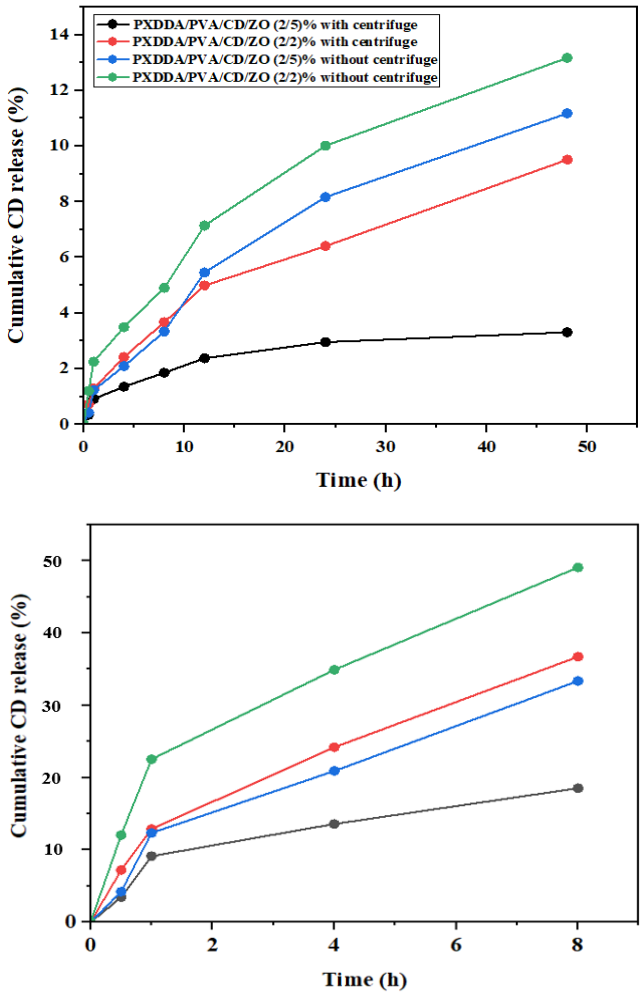

Figure 15 The drug release of PXDDA/PVA/CD/ZO (2/2) %, and PXDDA/PVA/CD/ZO (2/5) % nanofibers in the states of centrifuged capsule and without centrifuged capsule during 48h

Table 4 Kinetic release of CD from samples

Samples	Zero-order kinetic model		First-order kinetic model		Higuchi model		Korsemeyer-Peppas model		
	K_0	R^2	K_t	R^2	K_{HC}	R^2	n	K_{KP}	R^2
1	11.753	0.9368	0.0194	0.6808	17.789	0.9959	0.5587	3.8414	0.9942
2	3.4882	0.767	0.0148	0.5217	24.661	0.9313	0.4679	3.5836	0.9239
3	16.476	0.9218	0.0181	0.7022	7.3416	0.9902	0.5112	4.0629	0.9844
4	15.042	0.9363	0.024	0.6484	69.25	0.9861	0.6998	3.7105	0.9703

3-3-7 Antibacterial properties of nanofibers

The antibacterial evaluation demonstrated that incorporating CD/ZO capsules into the PXDDA/PVA nanofibers significantly enhanced their antimicrobial performance against both S. aureus (Figure 16). The pure PXDDA/PVA nanofibers showed no inhibition zone, confirming that the polymer matrix itself possesses no intrinsic antibacterial activity. In contrast, all samples containing CD/ZO capsules exhibited distinct inhibition zones, indicating effective release of clindamycin and strong antibacterial function. Nanofibers containing non-centrifuged capsules produced the largest inhibition zones, which can be attributed to the presence of free, non-entrapped drug molecules that diffused rapidly into the medium. This observation is consistent with the release profiles showing a pronounced burst release for these samples. Conversely, nanofibers prepared with centrifuged capsules displayed smaller but more uniform and sustained inhibition zones. The centrifugation step effectively removed unbound drug, ensuring that only drug molecules strongly adsorbed or entrapped within the zeolite remained. As a result, clindamycin was released gradually through the zeolite pores and crosslinked nanofiber network, producing controlled and prolonged antibacterial activity. Increasing the capsule content from 2% to 5% enhanced antibacterial performance in both centrifuged and non-centrifuged samples, likely due to the higher drug-loading capacity and increased availability of clindamycin.

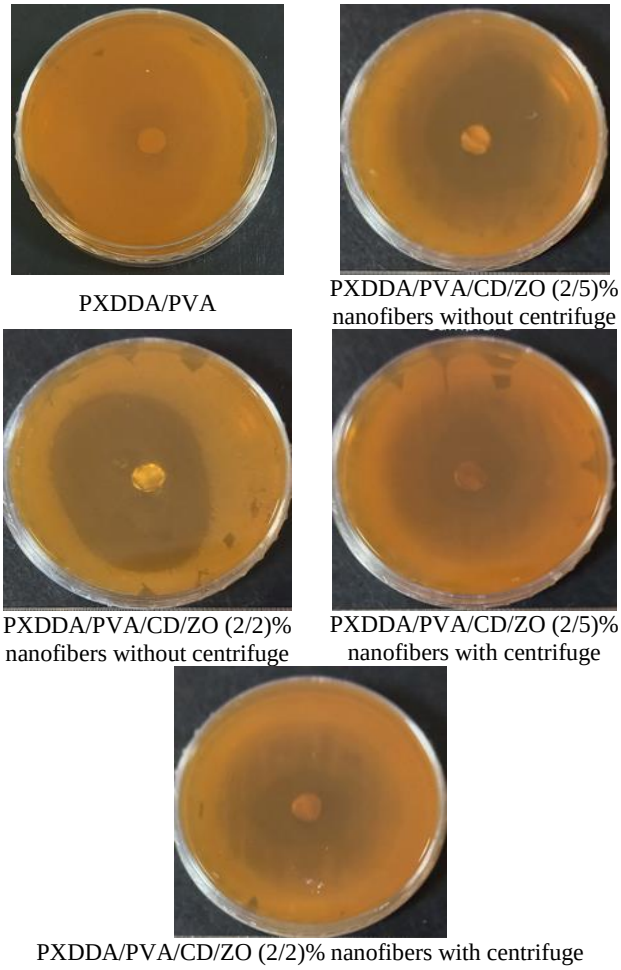

Figure 16 Antibacterial properties of nanofibers against S.aureus bacteria

3-3-8 Cell culture and MTT assay

Cell viability of the crosslinked nanofibers is presented in Figure 17. All samples exhibited relatively high levels of viability, with the PXDDA/PVA/CD/ZO (2/5)% sample without centrifugation showing the highest value, exceeding 130% at 24 h. This enhanced early-stage proliferation can be attributed not only to favorable surface characteristics and the absence of centrifugal compaction but also to the presence of glutaraldehyde crosslinking, which stabilizes the nanofiber structure and prevents rapid degradation that could otherwise negatively influence the cellular environment. Samples prepared without centrifugation generally demonstrated higher viability than the centrifuged ones at this stage, while the lowest value corresponded to the centrifuged (2/2)% sample, which remained above 40%, confirming acceptable cytocompatibility. At 48 h, a general decrease in viability was observed across most groups, indicating the transition toward a stabilization phase in cell adhesion and proliferation. The centrifuged (2/5)% formulation retained the highest viability (~88%), suggesting that, in combination with glutaraldehyde crosslinking, centrifugation improves structural uniformity and contributes to a more supportive microenvironment for long-term cellular interactions. In contrast, the PXDDA/PVA control and the (2/2%) non-centrifuged sample showed sharper declines, implying weaker support for sustained cell growth. At 72 h, the differences among formulations became more pronounced. The centrifuged (2/5)% nanofibers again showed the highest viability, exceeding 115%, confirming strong biocompatibility and stable long-term cell–material interactions. Both (2/2)% samples, centrifuged and non-centrifuged, displayed reduced viability at this stage, suggesting that the lower ZO content provides a less favorable environment for prolonged proliferation. The control PXDDA/PVA sample exhibited the lowest viability, further reinforcing the beneficial role of CD/ZO incorporation. It is important to emphasize that all nanofiber samples were crosslinked using glutaraldehyde, which significantly contributed to maintaining structural stability in the aqueous cellular environment. Crosslinking reduces premature dissolution and prevents the release of acidic degradation products, thereby supporting healthier cell growth and attachment. Moreover, nanofibers containing 5% ZO particles (Figure 18) provided the highest degree of cell adhesion, which is consistent with the improved viability observed in samples with higher ZO content.

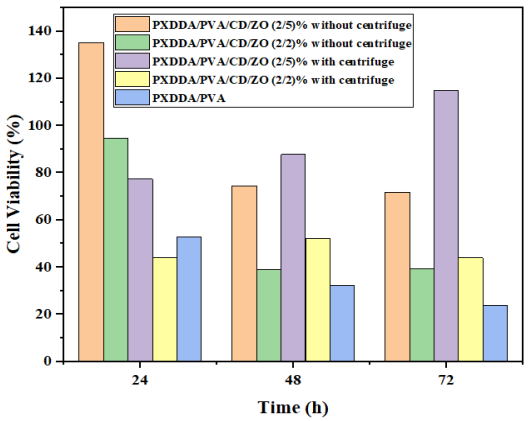

Figure 17 MTT assay of samples including PXDDA/PVA crosslinked nanofibers with capsules in different ratios of ZO for loading CD into them in the states of centrifuged and non-centrifuged

Overall, the results highlight that the (2/5)% CD/ZO ratio, especially when combined with centrifugation and glutaraldehyde crosslinking, offers the most favorable conditions for sustained cell viability due to improved mechanical integrity, structural uniformity, and optimized distribution of bioactive components.

PXDDA/PVA

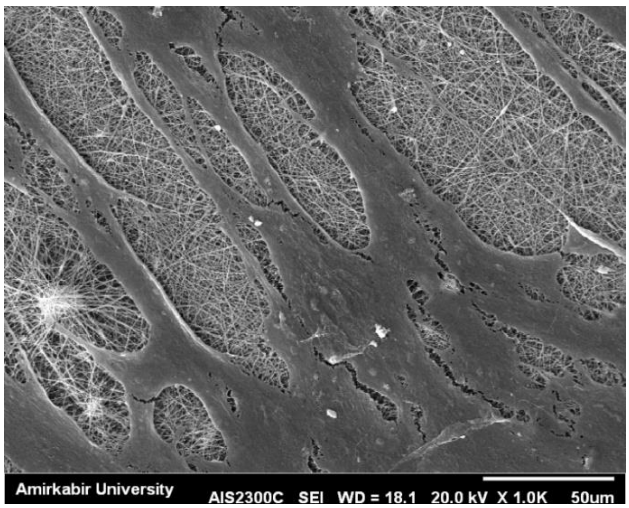

PXDDA/PVA/CD/ZO (2/2)%

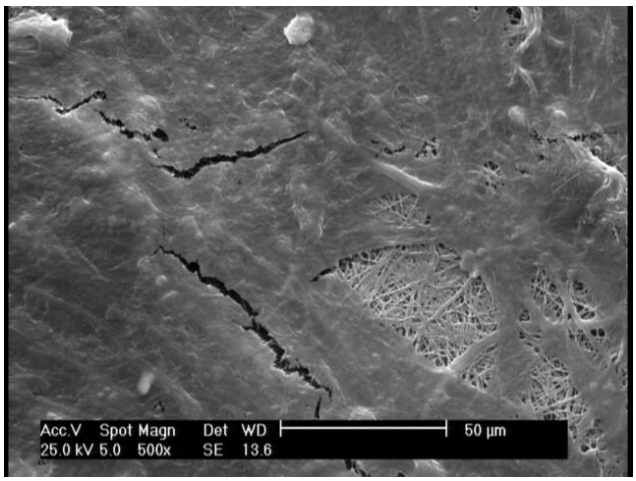

PXDDA/PVA/CD/ZO (2/5)%

Figure 18 Cell attachment of MSCs on nanofibers

4 Conclusion

In this study, the structural characteristics, drug-release behavior, and cytocompatibility of PXDDA/PVA/CD/ZO composite systems were systematically evaluated to determine the influence of composition and centrifugation on their performance. The results demonstrated that both the CD/ZO ratio and the application of centrifugation play critical roles in regulating material properties. Capsules prepared without centrifugation exhibited faster and higher cumulative CD release due to their less compact internal structure, whereas centrifuged samples provided a more controlled and sustained release profile. Moreover, the cytotoxicity assessment confirmed that all samples possessed acceptable biocompatibility, with the PXDDA/PVA/CD/ZO (2/5)% centrifuged sample supporting the highest long-term cell viability. Overall, the findings highlight that optimizing both samples ratio and processing conditions is essential for achieving desirable drug-release kinetics and enhanced biological performance, making these composite systems promising candidates for controlled drug delivery applications.

REFERENCES

[1] Khan MUA, Stojanović GM, Abdullah MFB, Dolatshahi-Pirouz A, Marei HE, Ashammakhi N, et al. Fundamental properties of smart hydrogels for tissue engineering applications: A review. International Journal of Biological Macromolecules. 2024;254:127882.

[2] Hsiung N, Ju Y, Yang K, Yang P, Zeng W, Zhao H, et al. Organoid-based tissue engineering for advanced tissue repair and reconstruction. Materials Today Bio. 2025:102093.

[3] Khan MUA, Aslam MA, Abdullah MFB, Hasan A, Shah SA, Stojanović GM. Recent perspective of polymeric biomaterial in tissue engineering–a review. Materials Today Chemistry. 2023;34:101818.

[4] Shah J, Patel D, Rananavare D, Hudson D, Tran M, Schloss R, et al. Recent advancements in chitosan-based biomaterials for wound healing. Journal of functional biomaterials. 2025;16(2):45.

[5] Rahmati M, Mills DK, Urbanska AM, Saeb MR, Venugopal JR, Ramakrishna S, et al. Electrospinning for tissue engineering applications. Progress in Materials Science. 2021;117:100721.

[6] Cho Y, Baek JW, Sagong M, Ahn S, Nam JS, Kim ID. Electrospinning and nanofiber technology: fundamentals, innovations, and applications. Advanced Materials. 2025;37(28):2500162.

[7] Basu B, Dutta A, Ash D, Garala K, Singh S, Prajapati BG. Recent advancements in the diagnosis and management of cancer using biomaterials-fabricated nanofibers: a review. Current medicinal chemistry. 2025;32(22):4376-400.

[8] Li X, Wang S, Zheng M, Ma Z, Chen Y, Deng L, et al. Synergistic integration of MXene nanostructures into electrospun fibers for advanced biomedical engineering applications. Nanoscale Horizons. 2024.

[9] Firoozi N, Kang Y. A highly elastic and autofluorescent poly (xylitol-dodecanedioic acid) for tissue engineering. ACS Biomaterials Science & Engineering. 2019;5(3):1257-67.

[10] Sotoudeh A, Darbemamieh G, Goodarzi V, Shojaei S, Asefnejad A. Tissue engineering needs new biomaterials: Poly (xylitol-dodecanedioic acid)–co-polylactic acid (PXDDA-co-PLA) and its nanocomposites. European Polymer Journal. 2021;152:110469.

[11] Dizaji BF, Azerbaijan MH, Sheisi N, Goleij P, Mirmajidi T, Chogan F, et al. Synthesis of PLGA/chitosan/zeolites and PLGA/chitosan/metal organic frameworks nanofibers for targeted delivery of Paclitaxel toward prostate cancer cells death. International Journal of Biological Macromolecules. 2020;164:1461-74.

[12] Hosseinzadeh H, Derafshi R, Mohammadi F, Abazari F, Hosseinzadeh M, Giti R. Soft Liners Loaded with Fluconazole Solid Lipid Nanoparticles (SLNs) and Clindamycin Niosomes as Drug Delivery Systems. BioNanoScience. 2025;15(3):1-13.

[13] Zamani M, Rodriguez DML, Zhang Z, Sabatini C, Swihart MT, Visser MB, et al. Synthesis of polymer-clindamycin conjugates through lipase-catalyzed esterification and RAFT polymerization. Polymer. 2025;317:127965.

[14] Voicu SI, Pandele AM, Nicoara AI, Antoniac IV, Oprea M, Bica C. Chitosan–Hydroxyapatite Composite Membranes for the Controlled Release of Clindamycin Phosphate to Prevent Infections at the Implantation Site. Ceramics. 2025;8(4):138.

[15] Nadem S, Ziyadi H, Hekmati M, Baghali M. Cross-linked poly (vinyl alcohol) nanofibers as drug carrier of clindamycin. Polymer Bulletin. 2020;77(11):5615-29.

[16] Alifah N, Palungan J, Ardayanti K, Ullah M, Nurkhasanah AN, Mustopa AZ, et al. Development of clindamycin-releasing polyvinyl alcohol hydrogel with self-healing property for the effective treatment of biofilm-infected wounds. Gels. 2024;10(7):482.

[17] Ranjbar N, Kolahdoozan M, Ebadi-Dehaghani H. Electrospun polycaprolactone/gelatin mat incorporated with glucosamine-loaded zeolite imidazolate framework-8 nanoparticles for cartilage tissue engineering. Journal of Polymer Research. 2024;31(1):9.

[18] Iqbal N, Kadir MRA, Mahmood NHB, Yusoff MFM, Siddique JA, Salim N, et al. Microwave synthesis, characterization, bioactivity and in vitro biocompatibility of zeolite–hydroxyapatite (Zeo–HA) composite for bone tissue engineering applications. Ceramics International. 2014;40(10):16091-7.

[19] Jiang B, Yang Z, Shi H, Jalil AT, Saleh MM, Mi W. Potentiation of Curcumin-loaded zeolite Y nanoparticles/PCL-gelatin electrospun nanofibers for postsurgical glioblastoma treatment. Journal of Drug Delivery Science and Technology. 2023;80:104105.

[20] Haghdoost F, Bahrami SH, Barzin J, Ghaee A. Preparation and characterization of electrospun polyethersulfone/polyvinylpyrrolidone-zeolite core–shell composite nanofibers for creatinine adsorption. Separation and Purification Technology. 2021;257:117881.

[21] Revathi S, Dey N, Thangaleela S, Vinayagam S, Gnanasekaran L, Sundaram T, et al. Nanocarrier optimization: Encapsulating Hydrastis canadensis in chitosan nanoparticles for enhanced antibacterial and dye degradation performance. International Journal of Biological Macromolecules. 2024:133316.

[22] Rabbi A, Nasouri K, Bahrambeygi H, Shoushtari AM, Babaei MR. RSM and ANN approaches for modeling and optimizing of electrospun polyurethane nanofibers morphology. Fibers and Polymers. 2012;13:1007-14.

[23] Shokrollahi M, Bahrami SH, Nazarpak MH, Solouk A. Multilayer nanofibrous patch comprising chamomile loaded carboxyethyl chitosan/poly (vinyl alcohol) and polycaprolactone as a potential wound dressing. International journal of biological macromolecules. 2020;147:547-59.

[24] Li S, Yang H, Wang S, Wang J, Fan W, Dong M. Improvement of adsorption and catalytic properties of zeolites by precisely controlling their particle morphology. Chemical Communications. 2022;58(13):2041-54.

[25] Haghbin M, Malekshah RE, Sobhani M, Izadi Z, Haghshenas B, Ghasemi M, et al. Fabrication and characterization of Persian gum-based hydrogel loaded with gentamicin-loaded natural zeolite: An in vitro and in silico study. International journal of biological macromolecules. 2023;235:123766.

[26] Mohandesnezhad S, Pilehvar-Soltanahmadi Y, Alizadeh E, Goodarzi A, Davaran S, Khatamian M, et al. In vitro evaluation of Zeolite-nHA blended PCL/PLA nanofibers for dental tissue engineering. Materials Chemistry and Physics. 2020;252:123152.

[27] Guo C, Wang S, Zhang S, Wang X, Guo H. The structure and packaging properties of films made by Poly (lactic acid)/lactide grafted Zeolite. Journal of Membrane Science. 2024;690:122227.

[28] Kiradzhiyska D, Batsalova T, Dzhambazov B, Milcheva N, Gavazov K, Zahariev N, et al. Synthesis, Characterization, and Cytotoxicity Evaluations of Silver–Zeolite Nanocomposite. Coatings. 2024;14(6):681.

[29] Bahi A, Shao J, Mohseni M, Ko FK. Membranes based on electrospun lignin-zeolite composite nanofibers. Separation and Purification Technology. 2017;187:207-13.